

Article

RETRACTED: Nanoformulated Ajwa (Phoenix Dactylifera) Bioactive Compounds Improve the Safety of Doxorubicin without Compromising Its Anticancer Efficacy in Breast Cancer

Kavitha Godugu ¹, Ali H. El-Far ² , Soad Al Jaouni ³ and Shaker A. Mousa ^{1,*} 

¹ Pharmaceutical Research Institute, Albany College of Pharmacy and Health Sciences, Rensselaer, NY 12144, USA; Kavitha.Godugu@acphs.edu

² Department of Biochemistry, Faculty of Veterinary Medicine, Damanhour University, Damanhour 22511, Egypt; ali.elfar@damanhour.edu.eg

³ Department of Hematology/Pediatric Oncology, Yousef Abdulatif Jameel Scientific Chair of Prophetic Medicine Application, Faculty of Medicine, King Abdulaziz University, Jeddah 21589, Saudi Arabia; saljaouni@kau.edu.sa

* Correspondence: shaker.mousa@acphs.edu; Tel.: +1-518-694-7397; Fax: +1-518-694-7567

Academic Editor: Tamer Elbayoumi

Received: 8 May 2020; Accepted: 26 May 2020; Published: 3 June 2020;

Corrected: 9 December 2022; Retracted: 30 April 2025



Abstract: One of the major causes of women's death in the world is breast cancer. Consequently, numerous regimens for the control of this severe disease have been created. The chemotherapeutic agent doxorubicin (DOX) is frequently used to treat breast cancer, but DOX can also cause cardiotoxic effects that lead to heart failure. Therefore, many research studies have been done to find a natural product that effectively potentiates or does not interfere with DOX's anticancer effect and protects against its cardiotoxicity. We studied the impact of combined nanoformulated Ajwa (Phoenix dactylifera) selected bioactive compounds (BAC) rutin (R) and quercetin (Q) in nude mice breast cancer xenografts on DOX-mediated anticancer efficacy. We also studied if this Ajwa BAC could safeguard against DOX-mediated cardiomyopathies by evaluating plasma cardiac troponin-I (cTn-I) levels and cardiac histopathology. Nanoformulated Ajwa BAC effectively alleviated weight loss induced by DOX in mice and significantly decreased the elevated cTn-I. Furthermore, 5 mg RQ-NPs/kg of nude mice that subcutaneously daily injected for 11 days, attenuated the histopathological alterations induced in cardiac muscles due to DOX without any interference with the anticancer effects of DOX against breast cancer.

Keywords: Ajwa bioactive ingredients; rutin; quercetin; nanoformulation; doxorubicin; anticancer efficacy; breast cancer; cardiomyopathy

1. Introduction

Breast cancer is the most common malignancy among women and is a major public health problem [1]. The MCF7 cell line is a frequently used cell line of breast cancer and was originally isolated from the pleural effusion of a 69-year-old woman with metastatic disease [2]. The use of the MCF7 cell line has produced more practical data for patient care than any other cell line of breast cancer [3]. It is estrogen receptor (ER)-positive and progesterone receptor (PR)-positive [4]. Furthermore, MCF7 is a poorly aggressive and non-invasive cell line [5], usually thought of as having poor metastatic ability [4].

The chemotherapeutic drug doxorubicin (DOX) causes anticancer activity by the induction of DNA damage and the production of reactive oxygen species (ROS) [6], which lead to cell cycle arrest

and other senescence biomarkers [7,8]. One of the most interesting ways to treat metastatic breast cancer is through DOX-based regimens [9,10]. DOX is also the most efficient and frequently used anthracycline drug against multiple malignancies. Unfortunately, its clinical application is limited by dose-based and essentially irreversible cardiotoxicity, leading to cardiomyopathy and congestive heart failure [11].

Phoenix dactylifera contains many phytochemical constituents including phenolics and flavonoids such as quercetin (Q) and rutin (R). Besides its nutritional role, *P. dactylifera* contains amino acids, carbohydrates, vitamins, and minerals [12]. Ajwa dates are a special type of *P. dactylifera* that is chiefly cultivated in Al-Madina Al-Munawwarah, Saudi Arabia [13]. The anticancer effect of Ajwa-dates has been reported against MCF7 [14] and human hepatocellular carcinoma (HepG2) cells [15] in vitro by inducing apoptosis and cell cycle arrest.

Cancer nano-therapy is growing rapidly and is being implemented to overcome many shortcomings of drugs such as non-specific targeting, water solubility inadequacy, and low oral bioavailability [16]. Nanoformulation enhances the delivery of natural compounds to fight cancer [17–19]. Natural therapy in combination with chemotherapy has long been used in cancer therapy to both improve the anticancer effects of chemotherapy and to counter its side effects [20]. Therefore, the current study investigated the potential effect of nanoformulated Ajwa bioactive compounds (BAC), namely R and Q, on DOX anticancer efficacy and safety (DOX-mediated cardiac toxicity) in transplanted MCF7 breast cancer.

2. Results

2.1. RQ-NPs Size and Entrapping Efficiency

The size distribution of RQ-NPs in aqueous solution was 200 nm (Figure 1), and the entrapment efficiency of the RQ-NPs was found to be around 70%.

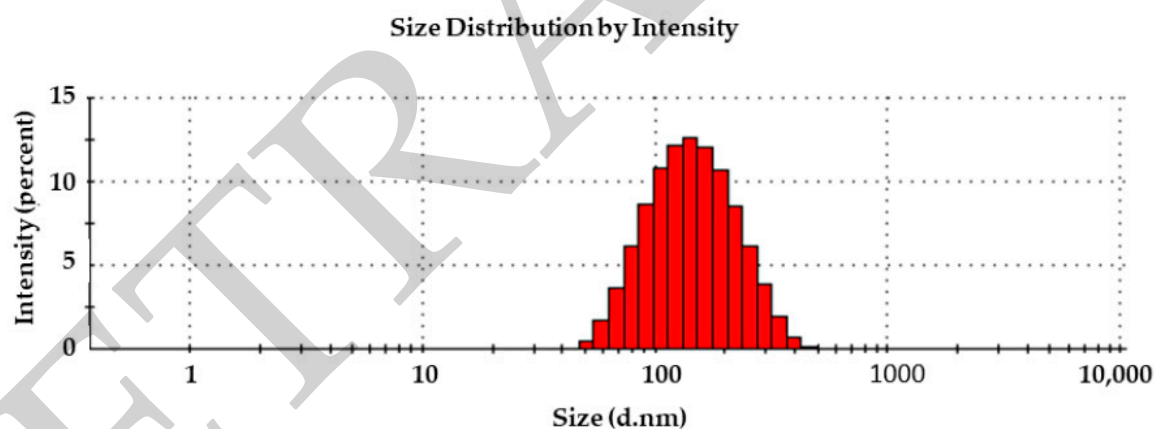


Figure 1. Size measurement of rutin-quercetin NPs (RQ-NPs) using dynamic light scattering (DLS). Average particle size is around 200 nm in diameter: Polydispersity index (PDI) = 0.169.

2.2. Effect of DOX and RQ-NPs on Body Weight

There were no significant changes due to treatments with DOX, RQ-NPs, or their combination on the body weights of mice implanted with MCF7 cells (Figure 2).

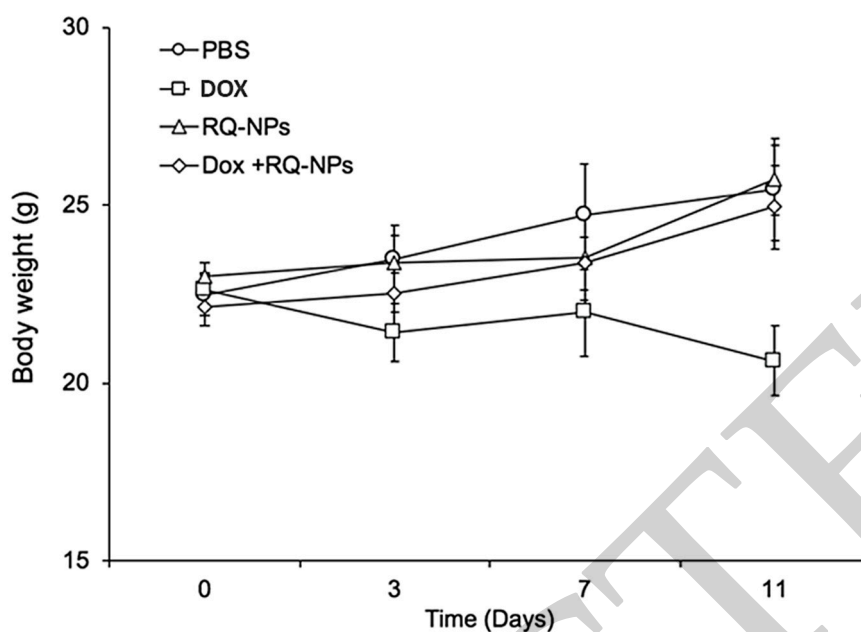


Figure 2. Effect of DOX + rutin and quercetin (RQ)-NPs, doxorubicin (DOX), and their combination on body weight (g). Values are expressed as the mean \pm SEM.

2.3. Effect of DOX and RQ-NPs on Tumor Volume

Tumor volumes (mm^3) of mice in the DOX treated group were significantly decreased on Days 7 and 11 ($p < 0.01$), while in the RQ-NP group, the tumor volumes had no differences in comparison with the control (Figure 3). The combination of DOX and RQ-NPs significantly decreased ($p < 0.01$) the tumor volume at Day 11 only when compared with the control. Generally, the tumor volume was significantly decreased for DOX ($p < 0.01$) and DOX + RQ-NP ($p < 0.01$) treated mice compared with the control group, while mice in the DOX group showed a significant ($p < 0.05$) reduction in tumor volume compared with DOX + RQ-NPs.

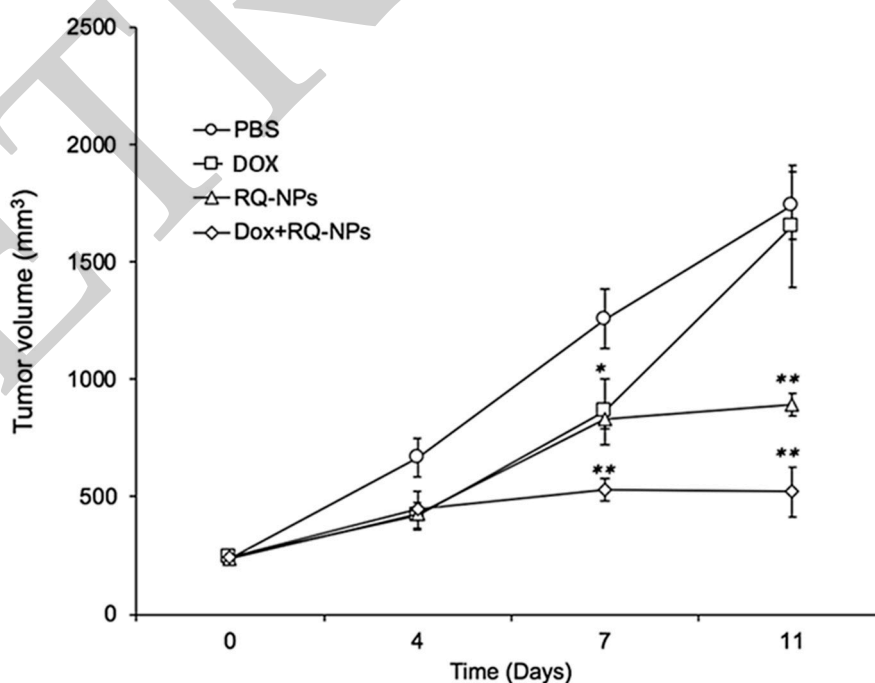


Figure 3. Effect of DOX + RQ-NPs, doxorubicin (DOX), and their combination on tumor volume (mm^3). Values are expressed as the mean \pm SEM. * $p < 0.05$, ** $p < 0.01$.

2.4. Effect of DOX and RQ-NPs on Tumor Weight

The results shown in Figure 4 revealed a significant reduction ($p < 0.01$) in tumor weight in the DOX and DOX + RQ-NPs groups in comparison with the control. Furthermore, both groups showed a significant reduction in tumor weight ($p < 0.01$) compared with the RQ-NP group.

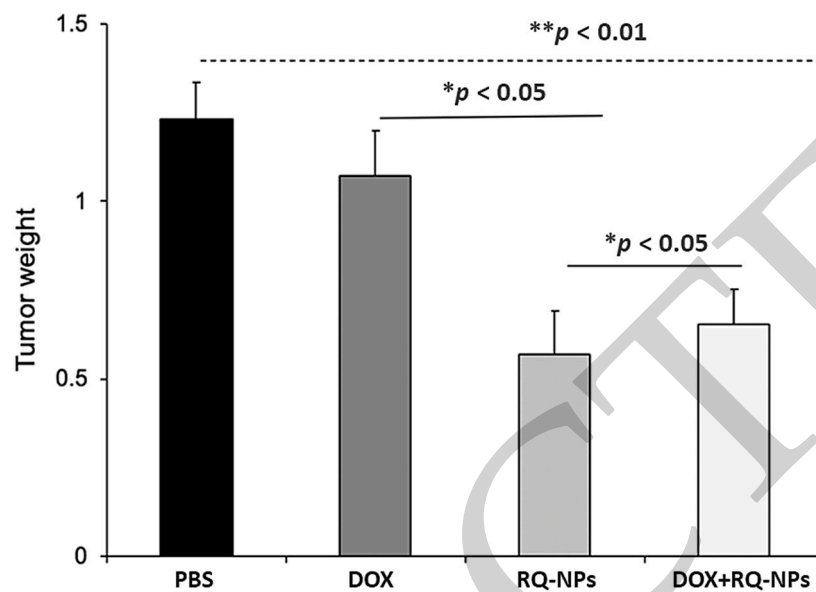


Figure 4. Effect of DOX + RQ-NPs, doxorubicin (DOX), and their combination on tumor weight (g). Values are expressed as the mean \pm SEM. * $p < 0.05$, ** $p < 0.01$.

2.5. Effect of DOX and RQ-NPs on Plasma cTn-I Levels

Mice in the RQ-NP group exhibited a significant reduction ($p < 0.05$) in plasma cTn-I levels (ng/mL) on Day 11 compared with Day 0 of the same group, while in the DOX and DOX + RQ-NP groups, there were significant increases ($p < 0.001$) in cTn-I levels. DOX + RQ-NP treated mice exhibited a significant decrease ($p < 0.01$) in cTn-I levels when compared with DOX treated mice (Figure 5).

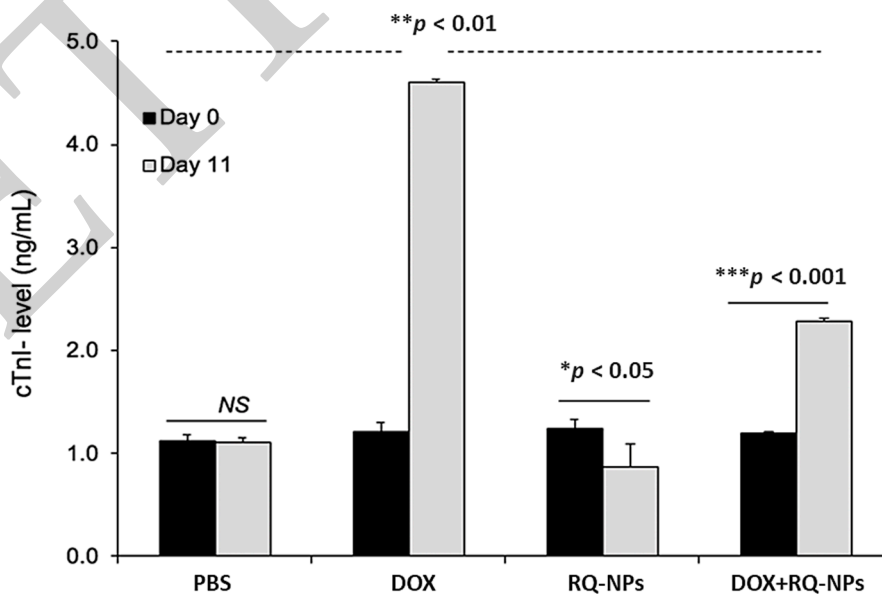


Figure 5. Effect of DOX + RQ-NPs, doxorubicin (DOX), and their combination on plasma troponin I levels (cTn-I). Values are expressed as the mean \pm SEM. * $p < 0.05$, ** $p < 0.01$, and *** $p < 0.001$. NS means nonsignificant.

2.6. Effect of DOX and RQ-NPs on Heart Histopathology

The RQ-NP treated group showed a normal myocardial morphology, approximately the same as the control (Figure 6). The cardiac morphology of DOX treated mice showed extensive cellular disarrangement, cytoplasmic vacuolization, and cell death, while in DOX + RQ-NP treated mice, the cardiomyocyte vacuolization was completely reduced with RQ-NP treatment.

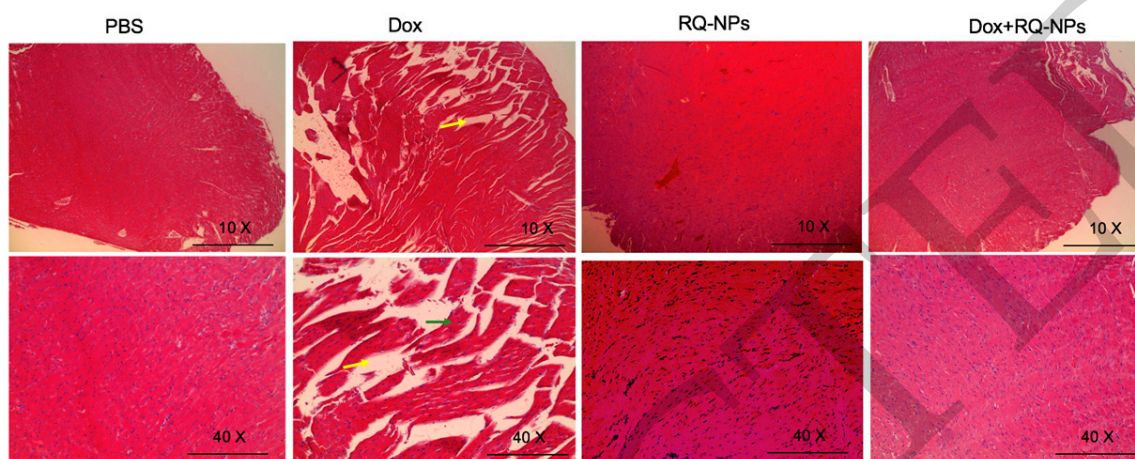


Figure 6. Effect of DOX + RQ-NPs, doxorubicin (DOX), and their combination on cardiac tissue histopathology. The control (PBS treated mice) shows normal myocardial morphology. RQ-NP treated mice show normal myocardial morphology. DOX treated mice show damaged hearts with extensive disarrangement, cytoplasmic vacuolization, and cell death (yellow arrows) with macrophage infiltration (green arrow). DOX + RQ-NP treated mice show that the cardiomyocyte vacuolization was completely reduced with Ajwa bioactive compound (BAC) treatment.

3. Discussion

DOX is an efficient chemotherapeutic anticancer therapeutic for many malignancies, including breast cancer. In the current study, DOX induced significant reductions in tumor volume and weight compared with control RQ-NPs, while in DOX + RQ-NPs, RQ-NPs did not induce a significant effect on DOX efficacy against MCF7 implantation in mice. On the contrary, some studies revealed a significant potentiation of DOX efficacy when Q was encapsulated with other nanoparticles. For example, Q enhanced DOX efficacy against DOX-resistant prostate cancer cells (PC-3/R) by downregulating the expression of the c-met and phosphoinositide 3-kinases/protein kinase B (AKT) pathway in vitro [21]. In addition, Q and DOX mesoporous silica nanoparticle encapsulation strengthened the DOX efficacy against gastric carcinoma (SGC7901/ADR) in vitro [22]. Chitosan, Q, and citraconic anhydride were formulated to enhance the anticancer effect of DOX on MCF7/ADR in vitro [23]. MCF7/ADR also demonstrated greater responsiveness to Q and DOX co-encapsulated with biotin receptor targeting nanoparticles both in vitro and in vivo [24]. Li et al. [25] stated that Q can increase intracellular accumulation of DOX in breast cancer cell lines (MCF7 and MDA-MB-231) by downregulating the expressions of P-gp, BCRP, and MRP1 expressions, thus potentiating DOX anticancer activity.

DOX is a cytotoxic drug commonly used in various procedures for chemotherapy. However, DOX induced severe side effects such as cardiotoxicity [26]. DOX accumulated in cardiac muscles' mitochondria because of its high affinity to cardiolipin, a phospholipid that is distinctively present in the inner mitochondrial membrane [27]. DOX mediated mitochondrial dysfunction caused by ROS and subsequently increased the oxidative stress that caused cardiomyopathies [28], observed by increased myocardial oxidized phospholipids [29] and elevated plasma cTn-I levels [30]. In the general sense of autophagy and mitophagy processes, DOX induced cardiotoxicity and cell mortality [26]. In the current study, Ajwa BAC significantly protected the cardiac muscles from the cardiomyopathy alterations that were induced by elevated ROS due to the antioxidant potential of Ajwa BAC active ingredients,

especially Q and R. The same results were achieved by Shi et al. [31], who reported that a combined DOX and Q treatment significantly increased the superoxide dismutase (SOD) activity and reduced the heart content of malondialdehyde (MDA), which counteracted DOX induced oxidative stress. Q treatment before DOX increased cell viability, SOD, catalase, and glutathione peroxidase activities and decreased MDA and ROS levels [32]. Q enhanced the antioxidant potential of cardiac muscle against DOX associated oxidative stress through significant increases in nuclear factor erythroid derived-2 mRNA expression [33]. Furthermore, Q protected mice had enhanced expression of Bmi-1 and antioxidative SOD against heart failure, followed by decreased ROS and lipid peroxidation [34]. On a proteomic analysis basis, Q attenuated oxidative changes in cardiomyocyte cells (H9c2) associated with DOX via the regulation of metabolic activation, protein folding, and cytoskeleton rearrangement [35].

Furthermore, R decreased heart failure caused by DOX by inhibiting autophagy and apoptosis by inhibition of AKT signaling [36]. Mandziuk et al. [37] observed a significant protective role of R against apoptotic and morphological changes induced by DOX in cardiomyocytes (H9c2).

4. Materials and Methods

4.1. Materials

The MCF7 (human breast cancer cell line) cell line was purchased from American Type Culture Collection (ATCC, Manassas, VA, USA). All cell culture reagents were purchased from Sigma-Aldrich (St. Louis, MO, USA). ELISA kits for measuring cardiac troponin-I (cTn-I) levels were obtained from Life Diagnostics, Inc. (West Chester, PA, USA). DOX and the Ajwa bioactive compounds R and Q were obtained from Sigma-Aldrich.

4.2. Cell Culture

MCF7 was cultured in Dulbecco's Modified Eagle Medium (DMEM) supplemented with 10% fetal bovine serum (FBS), 1% penicillin, and 1% streptomycin and maintained at 37 °C in an incubator with a humidifier atmosphere of 5% CO₂.

4.3. Nanoformulation, Characterization, and Entrapment Efficiency

R- and Q-nanoparticles (RQ-NPs) were synthesized by modifying a previously described method [38–40]. The optimized method of encapsulation of R/Q with poly(lactic-co-glycolic acid) (PLGA)/1, 2-distearoyl-sn-glycero-3-phosphoethanolamine-poly(ethylene glycol) (DSPE-PEG) nanoparticles involved dissolving 400 mg PLGA in 4 mL ethyl acetate. This solution was added to 20 mg of R + Q, 10 mg each, and mixed well. Finally, fifty microliters of DSPE-PEG (25 mg/mL) were added, and the solution was mixed again. The entire solution was added to 20 mL of 2% polyvinyl alcohol, and the resultant mixture was sonicated intermittently for 90 s. Ethyl acetate and the free R and Q were removed by dialysis. To the dialyzed solution using a dialysis membrane bag with a membrane cutoff of 6–8 kDa, one gram of sucrose was added (as a cryoprotectant), and the entire solution was freeze dried.

To assess the stability of RQ-NPs, samples were added to 5 mL glass vials, sealed with plastic caps, and placed in an accelerated stability chamber at a temperature of 37 °C ± 2 °C with a relative humidity of 65 ± 5%. The in vitro release kinetics of R/Q from the RQ-NPs were investigated with a dialysis method with fresh release medium. In brief, two milliliters of a solution of RQ-NPs or free R/Q were dissolved in PBS solution, added to a dialysis bag (molecular weight cutoff of 6–8 kDa), and dialyzed against 20 mL of release medium under gentle stirring with a paddle revolving at 100 rpm at a temperature of 37 °C. At designated time intervals, five-hundred microliter aliquots of external release media were withdrawn, after which the dialysis buffer was replenished with an equal volume of fresh medium and returned to suspension. The withdrawn medium was centrifuged at 5000× g for 5 min at 4 °C, and the supernatant content of released R/Q in the supernatant was determined with high-performance liquid chromatography (HPLC, Waters Corporation, Milford, MA, USA).

The size distribution of the synthesized nanoparticles (RQ-NPs) in aqueous dispersions was determined using a Malvern zeta sizer (Malvern Instrumentation Co, Westborough, MA, USA). Fifty milligrams of the lyophilized nanoparticles were resuspended in 2 mL of DI water and by placing this nanoparticle solution into a 3 mL, 4-sided, clear plastic cuvette and measured directly.

The amount of drug (R/Q) encapsulated in the nanoparticles was determined using ultraviolet–visible (UV-Vis) spectroscopy (Waters Corporation, Milford, MA USA) to measure R absorbance at λ 363 nm and Q absorbance at 557 nm and comparing with standard curves.

The amount of R/Q in the nanoparticles was determined by disintegrating the nanoparticles and measuring R/Q with UV-Vis spectroscopy. First, the amount of free R/Q (not encapsulated) was separated by filtering through a Millipore (Burlington, MA, USA) centrifugal device with a 3 kDa cut-off, assisted by centrifugation, at around 6500 rpm for 30 min. A measured known amount of RQ-NPs was disintegrated by adding an acetic acid solution. The entire solution was passed through the Millipore filtration centrifugal device and centrifuged as before to separate the R/Q. The R/Q concentration of the centrifugate/filtrate was then determined using a Nanodrop 2000C UV-Vis spectrophotometer (Thermo Fisher Scientific, Waltham, MA, USA).

The entrapment efficiency was determined with the following formula:

$$\text{Entrapment efficiency (loading)} = ([\text{Drug}]_f)/([\text{Drug}]_t) \times 100$$

where $[\text{Drug}]_f$ is the concentration of R or Q in the nanoparticles and $[\text{Drug}]_t$ is the theoretical concentration of the drug (meaning total amount of R/Q added initially).

4.4. Animals

Immune-deficient female Ncr nude homozygous mice (4–5 weeks of age, 15–20 g weight) were purchased from Taconic Biosciences, Inc. (Germantown, NY, USA). All animal studies were conducted at the animal facility of the Veteran Affairs Medical Center, Albany, NY, USA, in accordance with and approved by current institutional guidelines for humane animal treatment (Approval No.: 545,017 and Title: “Evaluation of Novel anticancer strategies in mouse model”). Mice were maintained under specific pathogen-free conditions and housed under controlled temperature (20–40 °C) and humidity (60–70%) and a 12 h light/dark cycle with ad libitum access to water and food. Mice were acclimatized for 5 days before the study.

4.5. Tumor Implantation and Treatment

Mice were orthotopically implanted in each flank with 2×10^6 cells suspended in 100 μL of media with 50% Matrigel[®] to achieve two independent tumors per animal. Immediately prior to initiation of treatments, animals were randomized into four groups (three animals in each group) by tumor volumes measured with Vernier calipers. DOX was dosed daily at 1 mg/kg body weight of mice by subcutaneous (SC) injection, at Day 4 after MCF7 cancer cell implantation (after detection of a palpable tumor mass) with or without treatment with 5 mg RQ-NPs/kg, SC daily for 11 consecutive days. After that, animals were sacrificed, and tumors were collected for determination of tumor weights.

4.6. Determination of cTn-I Levels

Mice were anesthetized using 2% isoflurane, and blood was collected from the retroorbital plexus on the day before surgery (Day 0) and at the end of the treatment (Day 11). Plasma was separated by centrifugation at $2000 \times g$ for 15 min and used to determine cTn-I levels.

4.7. Histopathological Examination

Heart specimens were fixed in 10% formalin and processed for paraffin sections of 4 μm thickness. Sections were stained with Hematoxylin and Eosin (H&E) and examined under a light microscope (Leica DM1000, Buffalo Grove, IL, USA).

4.8. Statistical Analysis

Results are expressed as the mean \pm standard deviation. Statistical differences between groups were assessed using the paired Student's *t*-test. $p < 0.05$ was considered as significant.

5. Conclusions

Our results revealed that nanoformulated Ajwa bioactive ingredients protected against body weight loss induced by DOX and did not interfere with DOX anticancer effects against MCF7 implanted cancer cells in this mouse model. Interestingly, nanoformulated Ajwa bioactive ingredients also protected the MCF7 implanted mice from the well-known myocardial pathology that is caused by DOX, as was evident from the reversal of the cardiac marker troponin I and cardiac tissue injury based on histopathological assessment.

Author Contributions: Conceptualization, K.G., A.H.E.-F., S.A.J., and S.A.M.; methodology, K.G., A.H.E.-F. and S.A.M.; software, K.G., A.H.E.-F., S.A.J.; validation, K.G., A.H.E.-F., S.A.J. and S.A.M.; formal analysis, K.G., A.H.E.-F., S.A.J.; investigation, K.G., A.H.E.-F. and S.A.M.; resources, S.A.J. and S.A.M.; data curation, K.G., A.H.E.-F., S.A.J. and S.A.M.; writing—original draft preparation, K.G., A.H.E.-F. and S.A.M.; writing—review and editing, K.G., A.H.E.-F. and S.A.M.; visualization, K.G., A.H.E.-F. and S.A.M.; supervision, S.A.J. and S.A.M.; project administration, S.A.J. and S.A.M.; funding acquisition, S.A.J. and S.A.M. All authors have read and agreed to the published version of the manuscript.

Funding: This research received no external funding.

Acknowledgments: We appreciate Dhruba Bharali's technical help with the nanoformulations and Kelly Keating for her editorial assistance.

Conflicts of Interest: All authors declare no potential conflicts of interest.

References

1. Comşa, Ş.; Cîmpean, A.M.; Raica, M. The story of mcf-7 breast cancer cell line: 40 years of experience in research. *Anticancer Res.* **2015**, *35*, 3147–3154. [[PubMed](#)]
2. Soule, H.D.; Vazquez, J.; Long, A.; Albert, S.; Brennan, M. A Human Cell Line From a Pleural Effusion Derived From a Breast Carcinoma 2. *Jnci J. Natl. Cancer Inst.* **1973**, *51*, 1409–1416. [[CrossRef](#)] [[PubMed](#)]
3. Sweeney, E.E.; McDaniel, R.E.; Maximov, P.Y.; Fan, P.; Jordan, V.C. Models and mechanisms of acquired antihormone resistance in breast cancer: Significant clinical progress despite limitations. *Horm. Mol. Biol. Clin. Investig.* **2012**, *9*, 143–163. [[CrossRef](#)] [[PubMed](#)]
4. Farshad, H.; Zarghi, A.; Kobarfard, F.; Zendehtdel, R.; Nakhjavani, M.; Arfaiee, S.; Zebardast, T.; Mohebi, S.; Anjidani, N.; Ashtarinezhad, A.; et al. Remarks in Successful Cellular Investigations for Fighting Breast Cancer Using Novel Synthetic Compounds. In *Breast Cancer—Focusing Tumor Microenvironment, Stem Cells and Metastasis*; InTech: Rijeka, Croatia, 2011.
5. Gest, C.; Joimel, U.; Huang, L.; Pritchard, L.-L.; Petit, A.; Dulong, C.; Buquet, C.; Hu, C.-Q.; Mirshahi, P.; Laurent, M.; et al. Rac3 induces a molecular pathway triggering breast cancer cell aggressiveness: Differences in MDA-MB-231 and MCF-7 breast cancer cell lines. *BMC Cancer* **2013**, *13*, 63. [[CrossRef](#)] [[PubMed](#)]
6. Gewirtz, D. A critical evaluation of the mechanisms of action proposed for the antitumor effects of the anthracycline antibiotics adriamycin and daunorubicin. *Biochem. Pharm.* **1999**, *57*, 727–741. [[CrossRef](#)]
7. Lord, C.J.; Ashworth, A. The DNA damage response and cancer therapy. *Nature* **2012**, *481*, 287–294. [[CrossRef](#)]
8. Lu, T.; Finkel, T. Free radicals and senescence. *Exp. Cell Res.* **2008**, *314*, 1918–1922. [[CrossRef](#)] [[PubMed](#)]
9. Carvalho, C.; Santos, R.; Cardoso, S.; Correia, S.; Oliveira, P.; Santos, M.; Moreira, P. Doxorubicin: The Good, the Bad and the Ugly Effect. *Curr. Med. Chem.* **2009**, *16*, 3267–3285. [[CrossRef](#)] [[PubMed](#)]
10. Toldo, S.; Goehe, R.W.; Lotrionte, M.; Mezzaroma, E.; Sumner, E.T.; Biondi-Zoccai, G.G.L.; Seropian, I.M.; Van Tassell, B.W.; Loperfido, F.; Palazzoni, G.; et al. Comparative Cardiac Toxicity of Anthracyclines In Vitro and In Vivo in the Mouse. *PLoS ONE* **2013**, *8*, e58421. [[CrossRef](#)]
11. Elliott, P. Pathogenesis of Cardiotoxicity Induced by Anthracyclines. *Semin. Oncol.* **2006**, *33*, 2–7. [[CrossRef](#)] [[PubMed](#)]
12. El-Far, A.H.; Oyinloye, B.E.; Sephehrimanesh, M.; Allah, M.A.G.; Abu-Reidah, I.; Shaheen, H.M.; Razeghian-Jahromi, I.; Alsenosy, A.E.-W.A.; Noreldin, A.E.; Al Jaouni, S.K.; et al. Date palm (phoenix

- dactylifera): Novel findings and future directions for food and drug discovery. *Curr. Drug Discov. Technol.* **2019**, *16*, 2–10. [[CrossRef](#)] [[PubMed](#)]
13. Rajab, A.R.; Elkablawy, M.A.; Sheik, B.Y. Antioxidant and Tissue-Protective Studies on Ajwa Extract: Dates from Al Madinah Almonwarah, Saudia Arabia. *Egypt. J. Forensic Sci. Appl. Toxicol.* **2012**, *12*, 201–223. [[CrossRef](#)]
 14. Khan, F.; Ahmed, F.; Pushparaj, P.N.; Abuzenadah, A.; Kumosani, T.; Barbour, E.; AlQahtani, M.; Gauthaman, K. Ajwa Date (Phoenix dactylifera L.) Extract Inhibits Human Breast Adenocarcinoma (MCF7) Cells In Vitro by Inducing Apoptosis and Cell Cycle Arrest. *PLoS ONE* **2016**, *11*, e0158963. [[CrossRef](#)] [[PubMed](#)]
 15. Siddiqui, S.; Ahmad, R.; Khan, M.A.; Upadhyay, S.; Husain, I.; Srivastava, A.N. Cytostatic and Anti-tumor Potential of Ajwa Date Pulp against Human Hepatocellular Carcinoma HepG2 Cells. *Sci. Rep.* **2019**, *9*, 245. [[CrossRef](#)]
 16. Dadwal, A.; Baldi, A.; Kumar Narang, R. Nanoparticles as carriers for drug delivery in cancer. *Artif. Cells Nanomed. Biotechnol.* **2018**, *46*, 295–305. [[CrossRef](#)]
 17. Mousa, D.S.; El-Far, A.H.; Saddiq, A.A.; Sudha, T.; Mousa, S.A. Nanoformulated Bioactive Compounds Derived from Different Natural Products Combat Pancreatic Cancer Cell Proliferation. *Int. J. Nanomed.* **2020**, *15*, 2259–2268. [[CrossRef](#)]
 18. Sudha, T.; El-Far, A.H.; Mousa, D.S.; Mousa, S.A. Resveratrol and Its Nanoformulation Attenuate Growth and the Angiogenesis of Xenograft and Orthotopic Colon Cancer Models. *Molecules* **2020**, *25*, 1412. [[CrossRef](#)]
 19. El-Far, A.; Al Jaouni, S.; Li, W.; Mousa, S. Protective Roles of Thymoquinone Nanoformulations: Potential Nanonutraceuticals in Human Diseases. *Nutrients* **2018**, *10*, 1369. [[CrossRef](#)]
 20. Bussing, A.; Bischof, M.; Hatzmann, W.; Bartsch, F.; Soto-Vera, D.; Fronk, E.-M.; Gmeindl, M. Prevention of surgery-induced suppression of granulocyte function by intravenous application of a fermented extract from *Viscum album* L. in breast cancer patients. *Anticancer Res.* **2005**, *25*, 4753–4757.
 21. Shu, Y.; Xie, B.; Liang, Z.; Chen, J. Quercetin reverses the doxorubicin resistance of prostate cancer cells by downregulating the expression of c-met. *Oncol. Lett.* **2017**, *15*, 2252–2258. [[CrossRef](#)]
 22. Fang, J.; Zhang, S.; Xue, X.; Zhu, X.; Song, S.; Wang, B.; Jiang, L.; Qin, M.; Liang, H.; Gao, L. Quercetin and doxorubicin co-delivery using mesoporous silica nanoparticles enhance the efficacy of gastric carcinoma chemotherapy. *Int. J. Nanomed.* **2018**, *13*, 5113–5126. [[CrossRef](#)] [[PubMed](#)]
 23. Mu, Y.; Wu, G.; Su, C.; Dong, Y.; Zhang, K.; Li, J.; Sun, X.; Li, Y.; Chen, X.; Feng, C. pH-sensitive amphiphilic chitosan-quercetin conjugate for intracellular delivery of doxorubicin enhancement. *Carbohydr. Polym.* **2019**, *223*, 115072. [[CrossRef](#)] [[PubMed](#)]
 24. Lv, L.; Liu, C.; Chen, C.; Yu, X.; Chen, G.; Shi, Y.; Qin, F.; Ou, J.; Qiu, K.; Li, G. Quercetin and doxorubicin co-encapsulated biotin receptor-targeting nanoparticles for minimizing drug resistance in breast cancer. *Oncotarget* **2016**, *7*, 32184–32199. [[CrossRef](#)] [[PubMed](#)]
 25. Li, S.; Yuan, S.; Zhao, Q.; Wang, B.; Wang, X.; Li, K. Quercetin enhances chemotherapeutic effect of doxorubicin against human breast cancer cells while reducing toxic side effects of it. *Biomed. Pharm.* **2018**, *100*, 441–447. [[CrossRef](#)] [[PubMed](#)]
 26. Koleini, N.; Kardami, E. Autophagy and mitophagy in the context of doxorubicin-induced cardiotoxicity. *Oncotarget* **2017**, *8*. [[CrossRef](#)] [[PubMed](#)]
 27. Wallace, K.B. Doxorubicin-Induced Cardiac Mitochondrionopathy. *Pharm. Toxicol.* **2003**, *93*, 105–115. [[CrossRef](#)]
 28. Kavazis, A.N.; Morton, A.B.; Hall, S.E.; Smuder, A.J. Effects of doxorubicin on cardiac muscle subsarcolemmal and intermyofibrillar mitochondria. *Mitochondrion* **2017**, *34*, 9–19. [[CrossRef](#)] [[PubMed](#)]
 29. Koleini, N.; Nickel, B.E.; Edell, A.L.; Fandrich, R.R.; Ravandi, A.; Kardami, E. Oxidized phospholipids in Doxorubicin-induced cardiotoxicity. *Chem. Biol. Interact.* **2019**, *303*, 35–39. [[CrossRef](#)]
 30. Morris, P.G.; Chen, C.; Steingart, R.; Fleisher, M.; Lin, N.; Moy, B.; Come, S.; Sugarman, S.; Abbruzzi, A.; Lehman, R.; et al. Troponin I and C-Reactive Protein Are Commonly Detected in Patients with Breast Cancer Treated with Dose-Dense Chemotherapy Incorporating Trastuzumab and Lapatinib. *Clin. Cancer Res.* **2011**, *17*, 3490–3499. [[CrossRef](#)]
 31. Shi, Y.; Su, X.; Cui, H.; Yu, L.; Du, H.; Han, Y. Combination of quercetin and Adriamycin effectively suppresses the growth of refractory acute leukemia. *Oncol. Lett.* **2019**. [[CrossRef](#)]

32. Chen, X.; Peng, X.; Luo, Y.; You, J.; Yin, D.; Xu, Q.; He, H.; He, M. Quercetin protects cardiomyocytes against doxorubicin-induced toxicity by suppressing oxidative stress and improving mitochondrial function via 14-3-3 γ . *Toxicol. Mech. Methods* **2019**, *29*, 344–354. [[CrossRef](#)] [[PubMed](#)]
33. Sharma, A.; Parikh, M.; Shah, H.; Gandhi, T. Modulation of Nrf2 by quercetin in doxorubicin-treated rats. *Heliyon* **2020**, *6*, e03803. [[CrossRef](#)] [[PubMed](#)]
34. Dong, Q.; Chen, L.; Lu, Q.; Sharma, S.; Li, L.; Morimoto, S.; Wang, G. Quercetin attenuates doxorubicin cardiotoxicity by modulating Bmi-1 expression. *Br. J. Pharm.* **2014**, *171*, 4440–4454. [[CrossRef](#)] [[PubMed](#)]
35. Chen, J.-Y.; Hu, R.-Y.; Chou, H.-C. Quercetin-induced cardioprotection against doxorubicin cytotoxicity. *J. Biomed. Sci.* **2013**, *20*, 95. [[CrossRef](#)]
36. Ma, Y.; Yang, L.; Ma, J.; Lu, L.; Wang, X.; Ren, J.; Yang, J. Rutin attenuates doxorubicin-induced cardiotoxicity via regulating autophagy and apoptosis. *Biochim. Biophys. Acta Mol. Basis Dis.* **2017**, *1863*, 1904–1911. [[CrossRef](#)]
37. Mandziuk, S.; Baj, T.; Sieniawska, E.; Dudka, J.; Gieroba, R.; Iwan, M.; Glowniak, K. Protective effect of Mutellina purpurea polyphenolic compounds in doxorubicin-induced toxicity in H9c2 cardiomyocytes. *Drug Chem. Toxicol.* **2015**, *38*, 1–8. [[CrossRef](#)]
38. Hariri, W.; Sudha, T.; Bharali, D.J.; Cui, H.; Mousa, S.A. Nano-Targeted Delivery of Toremifene, an Estrogen Receptor- α Blocker in Prostate Cancer. *Pharm. Res.* **2015**, *32*, 2764–2774. [[CrossRef](#)]
39. Bharali, D.J.; Sudha, T.; Cui, H.; Mian, B.M.; Mousa, S.A. Anti-CD24 nano-targeted delivery of docetaxel for the treatment of prostate cancer. *Nanomed. Nanotechnol. Biol. Med.* **2017**, *13*, 263–273. [[CrossRef](#)]
40. Siddiqui, I.A.; Bharali, D.J.; Nihal, M.; Adhami, V.M.; Khan, N.; Chamcheu, J.C.; Khan, M.I.; Shabana, S.; Mousa, S.A.; Mukhtar, H. Excellent anti-proliferative and pro-apoptotic effects of (–)-epigallocatechin-3-gallate encapsulated in chitosan nanoparticles on human melanoma cell growth both in vitro and in vivo. *Nanomed. Nanotechnol. Biol. Med.* **2014**, *10*, 1619–1626. [[CrossRef](#)]

Sample Availability: Samples of the compounds (RQ-NPs) are available from the authors.



© 2020 by the authors. Licensee MDPI, Basel, Switzerland. This article is an open access article distributed under the terms and conditions of the Creative Commons Attribution (CC BY) license (<http://creativecommons.org/licenses/by/4.0/>).